Supporting information

Decomposition of amyloid fibrils by NIR active upconversion nanoparticles

Takunori Harada[1,*], Hiraku Matsuzaki[1], Ryohei Oyama[1], Takuma Takeuchi[1], Tomoaki Takei[1], Taisuke Ninomiya[1], Kouta Takami[1], Takanori Inoue[1], Hiroyasu Nishiguchi[2], Emi Hifumi[2], Hiroyuki Shinto[3], Hiromi Takahashi[4] and Kazuo Umemura[5]

Table of Contents

1. Experimental Section

1.1 Materials, instrumentation and techniques

$YCl_3 \cdot 6H_2O$, $YbCl_3 \cdot 6H_2O$, $ErCl_3 \cdot 6H_2O$, branched polyethylenimine (PEI, 25 kDa), ethylene glycol (EG), and insulin (bovine pancreatic extract; M_w = 5733.49 g/mol) were purchased from Sigma-Aldrich. NaCl, NH_4F, eosin Y (EY), rose bengal (RB), orange G (OG), thioflavin T (ThT), methylene blue (MB), pseudoisocyanine (PIC), phenalenone (PN), and dextran sodium sulfate (DSS) were purchased from Wako Chemical Co. Ltd.. Anthracene-9,10-dipropionic acid disodium salt (ADPA) was purchased from Funakoshi Co. Ltd. All chemicals were used without further purification.

The crystalline structures of the UCNPs were analysed using X-ray powder diffraction (XRD), and the pattern given in Fig. S1 suggests that the nanoparticles are highly crystalline. Energy dispersive X-ray spectrometry (EDS) images were acquired using a field-emission scanning electron microscope (FE-SEM; JEOL JSM-7100F, Tokyo, Japan). The UCNPs nanoparticles were characterised by Ln-ion mapping in the core $NaYF_4$ particles using an EDS system attached to the FE-SEM.

In order to get more direct evidence for the particle size, the dispersed UCNPs was examined using Transmission electron microscopy (TEM) and dynamic light scattering (DLS) particle size analyzer. TEM images were recorded on a Hitachi H-7650 TEM (Tokyo, Japan). The TEM samples were prepared by dropping a suspension of nanoparticles on a carbon-film-coated copper grid (ELS-C10). Measurements of the zeta potential and particle-size distribution of the nanoparticles were performed on a ZetasizerNano ZS zeta-potential analyser (Malvern Panalytical, UK). Particles were diluted in deionised water and then sonicated for 5 min before sizing. The relative quantum efficiency was measured using a fluorescence spectrophotometer (FP-8600, Jasco) equipped with a 60-mm ϕ integral sphere (ISF-834).

Circular dichroism (CD) measurements were acquired using a chiroptical spectrophotometer (J-1500, Jasco) equipped with the capacity for obtaining true CD spectra, based on Stokes–Mueller matrix analysis.[1] The CD spectra were recorded over a wavelength range of 350–190 nm, using the ‘standard’ sensitivity setting and a scanning speed of 50 nm/min, with 1-nm resolution and time constant of 1 s. Data were further processed for noise reduction as necessary. Peptide secondary structure motif percentages were estimated with the CDPro software suite containing the SELCON3 and CONTIN/LL programs developed by Sreerama et al.[2]

Fluorescence and ultraviolet–visible (UV–vis) absorption measurements were performed using a spectrofluorometer (FP-8300: Jasco) and UV-Vis spectrophotometer (V-550: Jasco), respectively.

AFM observations were carried out by using a commercially available AFM (MFP-3D microscope, Asylum Research, CA, USA), equipped with a vertical-engage J scanner. A silicon cantilever (20–40 N/m; PPP-NCSTR-W, NANOSENSORS, NanoWorld AG, Neuchâtel, Switzerland) was used in tapping mode in air. Force values for imaging and scratching were estimated by force-curve measurements. Imaging in air was carried out in tapping or contact mode. The AFM unit was stored in a plastic chamber in which the humidity was controlled during measurements.

1.2 Synthetic procedure and characterization data

Synthesis I (UCNPs@PEI)

The synthesis of PEI-coated UCNPs (UCNPs@PEI) was performed by following a solvothermal procedure:[3–6] a 9.0 mL EG solution of NaCl (1.2 mM), YCl_3 (0.48 mM), $YbCl_3$ (0.108 mM), and $ErCl_3$ (0.012 mM) was mixed with 6 mL of a solution of 1.92-mM NH_4F in EG, and then PEI (0.45 mg) was added to the resulting mixture. The well-agitated transparent solution was transferred to a Teflon-lined autoclave (HU-25, SANAI Kagaku Co. Ltd.) and subsequently heated to 230 °C for 2.5 h, yielding a pale-yellow stock solution. Nanoparticles were collected by centrifugation; they were then washed in ethanol three times, and finally, placed in a drying oven for 2 h.

Synthesis II (Amyloid fibril)

Amyloid fibril (AF) formation without seeding was performed by a stepwise heating process.[7] Insulin was incubated at concentrations of 1.0 mg/mL, under a range of conditions, namely, in a solution of 25-mM HCl (pH 1.7) and 2.0-M NaCl and heated from room temperature to 92 °C at a constant rate of 2 °C/min. After the heating process, the sample temperature was lowered to room temperature. To remove non-reactant species, the obtained AF were collected by centrifugation and washed three times with glycine-NaOH buffer (pH 8.6)to yield AF stock solution.

Synthesis III (composite AF-UCNPs/PS)

PS was conjugated to the cationic UCNPs@PEI by electrostatic interactions. PS that was not coupled to UCNPs was separated from the PS-conjugated UCNPs by a series of washing steps involving centrifugation and resuspension in aqueous buffer solution. The AF–UCNP composite was produced in the presence of the previously prepared aqueous solution of PS-UCNPs (1.0 mL, 0.5 mg/mL, glycine–NaOH buffer, pH 8.6) by the addition of 1.0 mL of aqueous AF solution (0.17 mM). The electrostatic attraction between these two oppositely charged materials provides the driving force to form a stable AF/PS–UCNP complex. The stoichiometric ratio of AF to PS was adjusted in the range of 19–46:1 in a fixed UCNP concentration of 0.5 mg/mL. PS that was not coupled to UCNPs was separated from the PS-conjugated UCNPs by a series of washing steps involving centrifugation and resuspension in aqueous buffer solution.

Characterization

In order to obtain a more direct measurement of the particle size, the dispersed UCNPs were examined using transmission electron microscopy (TEM) and a dynamic light scattering (DLS) particle-size analyser. The TEM images were recorded using a Hitachi H-7650 TEM instrument (Tokyo, Japan). The TEM samples were prepared by dropping a suspension of nanoparticles onto a carbon-film-coated copper grid (ELS-C10, Okenshoji Co., Ltd., Tokyo, Japan). Fig. S2 displays TEM images that provide evidence that the individual NPs are spherical particles with approximate sizes of ~50–60 nm, in very good agreement with the DLS analysis.

In order to obtain direct evidence of the AF decomposition, the dispersed AF size distribution was examined using SDS-PAGE (Fig. S7 A and B). Native insulin, AF, and AF/UCNPs/PS are shown in lane 1, lane 2–3, and lane 4–5, respectively, and light and dark indicate the presence and absence,

106 respectively, of 30 min of NIR irradiation in Fig. S7 A and B. The strong intensity band at M_w = 3.5
107 kDa corresponds to the native insulin monomer, and some AF ladder bands are observed in the region
108 from 14.4 to 3.5 kDa in lanes 2 to 5. As shown in lane 5, for the UCNPs/AF composite with NIR
109 irradiation, a decrease in band intensities is clearly apparent, resulting in the decomposition of AF with
110 respect to the non-NIR irradiated sample (lane 4), although for the AF only (lane 2 and 3), no alteration
111 is observed upon the use of NIR irradiation. Therefore, it is could be assumed that the band intensities
112 belonging to AF with larger molecular weights (3.5–14.4 KDa) than that of native insulin (3.5 kDa)
113 decrease in because of the NIR-excited UCNPs@PEI/PS-mediated decomposition of AF to smaller-
114 sized fibrils via selective singlet O_2 attack. There is significant correspondence between these results
115 and those of the standard ThT fluorescence assay (Fig. 3). The heat effects of NIR irradiance ($1W/cm^2$),
116 e.g., decomposition of PS or AF and the lowering UC efficiency, were negligible small in our
117 experiments.
118

2. Figures

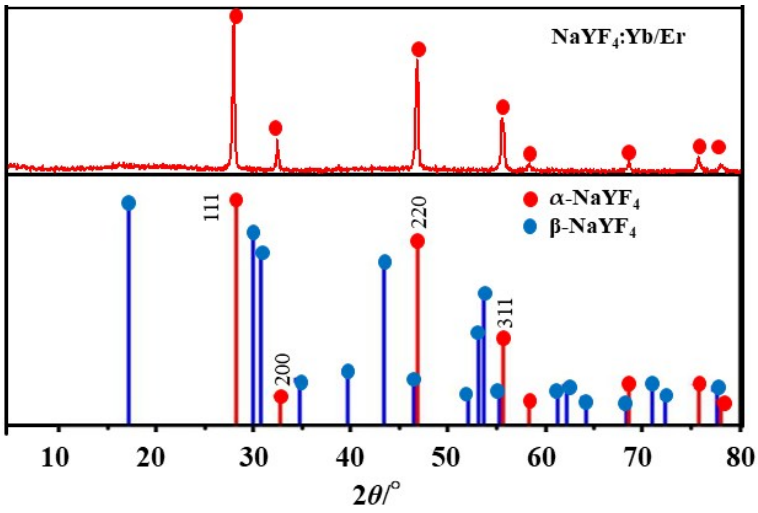

Figure S1. XRD patterns for the as-prepared $NaYF_4$:Yb/Er of (a) experimental patterns and (b) the standard spectral lines of α-$NaYF_4$ (JCPDS standard card No. 77-2042).

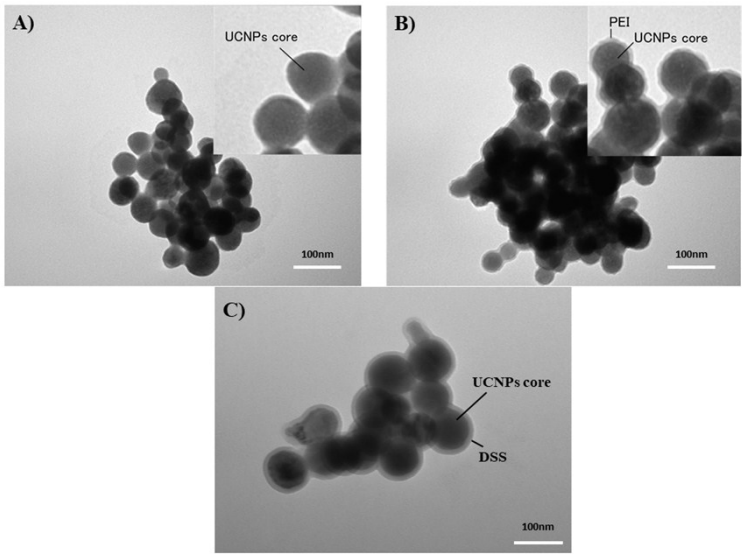

Figure S2. TEM image of $NaYF_4$:Yb/Er (18/2 mol%) nanocrystals. A) shows a typical TEM image of the bare $NaYF_4$:Yb/Er nanocrystals with an average diameter of 50 nm. B) These nanocrystals are uniform in size and bear a hydrophobic surface due to the capping of PEI on their surface. To make these nanocrystals suitable for conjugation, DSS layer is coated on their surface by a layer by layer (lbl) method.[8,9] The layers consist of PEI and DSS with a thickness of around 4.4 and 10.3 nm, as shown in the TEM image (2B and 2C). After DSS is grafted onto the PEI layer, the morphology of the core-shell nanoparticles is well maintained (2C), which suggests that the amino modification process has no side effect on the uniformity of the $NaYF_4$:Yb/Er nanoparticles. During the DSS modification process, the surface charge of the core-shell nanoparticles is altered from positive (ζ= +15 mV) to negative (ζ= −21 mV), confirming that the DSS have been successfully grafted onto these nanoparticles.

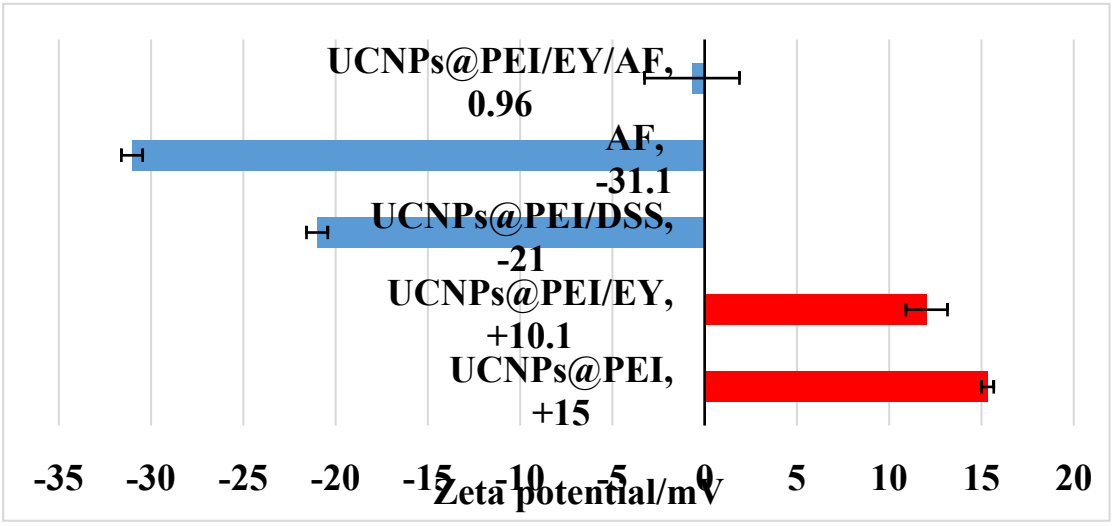

Figure S3. Zeta potential of UCNPs@PEI, PS-loaded UCNPs@PEI, UCNPs@PEI/DSS, amyloid fibril (AF) and AF-complexed UCNPs@PEI/PS. The error bars represent the standard deviation of three different experiments.

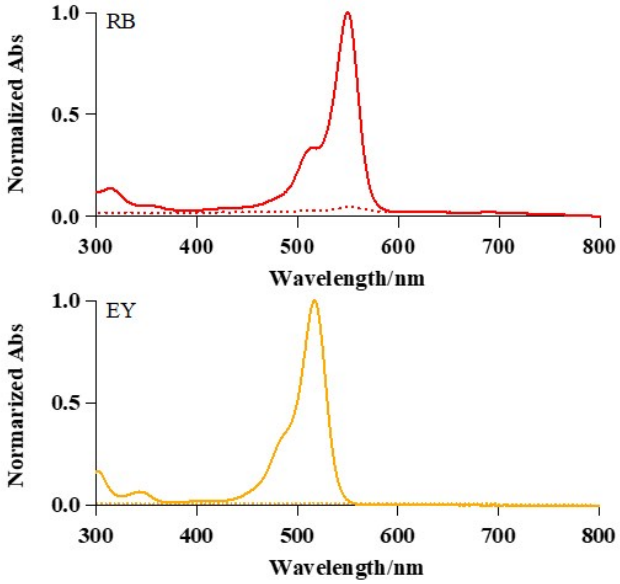

Figure S4. The electronic absorption spectra of UCNPs@PEI/PS composite and free PS in glycine-NaOH buffer (pH 8.6) desorbed from it: upper; RB, bottom; EY, solid line; UCNPs@PEI/PS solution at 0 hour just after hybridizing, dotted line; supernatant (free PS) desorbed the UCNPs@PEI/PS at 2 hours later.

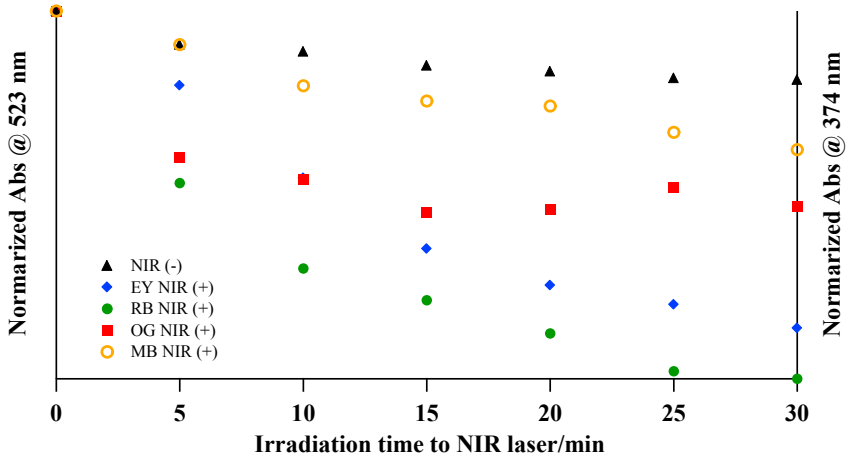

Figure S5. PIC and ADPA destruction representing singlet oxygen production (measured by absorption intensity at 523 and 374 nm) as a function of irradiation time to NIR laser (980 nm, 1 W/cm^2) shows steady fall from original (100 %) for the UCNPs@PEI/PS (EY, RB, OG and MB) with the irradiation in NIR laser (blue, green, red and orange) while UCNPs@PEI/PS (EY, RB, OG and MB) control undergoes slight bleaching without exposure to laser (black: average value for all PSs measurements), and absorption intensity for the solution containing only PS and $^1O_2$ agent was hardly changed (< 1 %) with the 30 min irradiation in NIR laser. PIC and ADPA were used as $^1O_2$-trapping agents in UCNPs@PEI/PS (EY, RB and OG) and UCNPs@PEI/PS (MB) measurements, respectively.

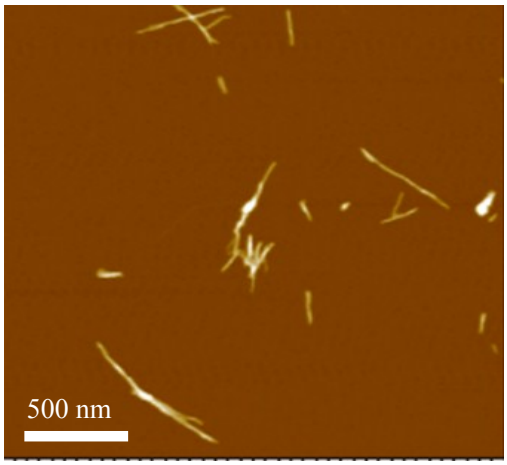

Figure S6. Tapping mode Atomic force microscopy (AFM) image of amyloid fibril (AF) on freshly cleaved mica: [insulin] = 0.17 mM. The scales bar indicates 500 nm. Sample was prepared for AFM by evaporating 3 μL of AF stock solution (at 25 °C) on fleshly cleaved mica. AFM observations were carried out with a commercially available AFM (MFP-3D microscope, Asylum Research, CA, USA), equipped with a vertical-engage J scanner. A silicon (20 to 40 N/m) cantilever was used for tapping mode in air.

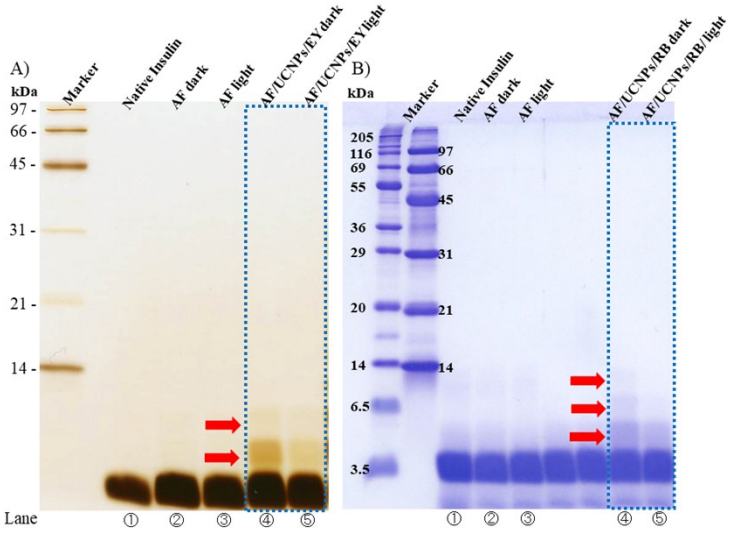

Figure S7. SDS-PAGE electrophoresis result for monitoring for amyloid fibril (AF): [insulin] = 0.17 mM. Marker lane contains approximately amount of Myosin, rabbit muscle (molecular mass 205 kDa), β-galactosidase, E.coli (116 kDa), phosphorylase B (97.4 kDa), Bovine serum albumin (69 kDa), bovine serum albumin (66.2 kDa), Glutamic dehydrogenase (55 kDa), chicken egg white ovalbumin (45 kDa), Lactic dehydrogenase,porcine muscle (36 kDa), carbonic anhydrase (31 kDa), Carbonic anhydrase, bovine liver (29 kDa), trypsin inhibitor (21.5 kDa), Trypsin inhibitor, soybean (20 kDa), lysozyme (14.4 kDa) Aprotinin, bovine lung (6.5 kDa) and Insulin B chain, bovine pancreas (3.5 kDa). AF fragments bands are indicated by arrows. The band intensities belonged to AF at larger bands than native insulin at 3.5 kDa bands decrease by the NIR-excited UCNPs@PEI/PS decomposition of AF to smaller size block fibrils due to the attack of singlet O_2 selectively.

3. References

1 T. Harada, *Polym. J*. 2018, **50**, 679.
2 N. Sreerama and R. W. Woody, *Anal. Biochem*., 2000, **287**, 252.
3 F. Wang and X. Liu, *J. Am. Chem. Soc*., 2008, **130**, 5642.
4 R. S. Niedbala, H. Feindt, K. Kardos, T. Vail, J. Burton, B. Bielska, S. Li, D. Milunic, P. Bourdelle and R. Vallejo, *Anal. Biochem*., 2001, **293**, 22.
5 P. Zhang, W. Steelant, M. Kumar and M. Scholfield, *J. Am. Chem. Soc*., 2007, **129**, 4526.
6 A. Sedlmeier and H. H. Gorris, *Chem. Soc. Rev*., 2015, **44**, 1526.
7 E. Chatani, H. Imamura, N. Yamamoto and M. Kato, *J. Biol. Chem*., 2014, **289**, 10399.
8 F. Wang and X. Liu, *Chem. Soc. Rev*., 2009, **38**, 976.
9 C. Graf, D. L. J. Vossen, A. Imhof and A. van Blaaderen, *Langmuir*, 2003, **19**, 6693.